Temperature distribution along the surface of evaporating droplets

Kai Zhang,[1] Liran Ma,[2] Xuefeng Xu,[1,*] Jianbin Luo,[2] and Dan Guo[2]
[1]*School of Technology, Beijing Forestry University, Beijing 100083, China*
[2]*State Key Laboratory of Tribology, Tsinghua University, Beijing 100084, China*
(Received 27 November 2013; revised manuscript received 13 February 2014; published 17 March 2014)

The surface temperature can significantly affect the flow field of drying droplets. Most previous studies assumed a monotonic temperature variation along the droplet surface. However, the present analyses indicate that a nonmonotonic spatial distribution of the surface temperature should occur. Three different patterns of the surface temperature distribution may appear during the evaporation process of liquid droplets: (i) the surface temperature increases monotonically from the center to the edge of the droplet; (ii) the surface temperature exhibits a nonmonotonic spatial distribution along the droplet surface; (iii) the surface temperature decreases monotonically from the center to the edge of the droplet. These surface temperature distributions can be explained by combining the evaporative cooling at the droplet surface and the heat conduction across the substrate and the liquid. Furthermore, a "phase diagram" for the distribution of the surface temperature is introduced and the effect of the spatial temperature distribution along the droplet surface on the flow structure of the droplet is discussed. The results may provide a better understanding of the Marangoni effect of drying droplets and provide a potential way to control evaporation-driven deposition as well as the assembly of colloids and other materials.

DOI: 10.1103/PhysRevE.89.032404 PACS number(s): 68.03.Cd, 68.03.Fg, 47.55.pf, 47.55.dm

I. INTRODUCTION

When a liquid droplet dries on a solid surface, the particles suspended in the droplet will deposit on the substrate and form different deposition patterns, e.g., a ring at the drop periphery, a central bump, and a uniform deposit [1–8]. This phenomenon has been used as the basis of a wide range of industrial and scientific applications involving particle deposition, including the deposition of DNA-RNA mapping [9–11], the ink-jet printing of functional materials [12–15], and disease diagnosis [16]. Controlling the distribution of deposition from evaporating droplets plays a vital role in these applications.

Among the factors involved, the convective Marangoni flow inside drying droplets can significantly influence the resulting patterns of deposition [1–6,17] and thus has motivated extensive theoretical and experimental research in recent years [18–26]. The surface temperature gradient of evaporating droplets generates convective flow and consequently alters the deposition pattern. Therefore, a better understanding of the temperature distribution along the surface of drying droplets will be important both in fundamental research and in practical applications.

While extensive theoretical and experimental research has been conducted on evaporating droplets in recent years [27–39], the spatial distribution of the surface temperature remains poorly understood because of the intersection of many related factors, e.g., the thermal conductivities of the liquid and the solid substrate [40], the microstructure at the droplet edge [22], and the heating substrate size [41]. Two opposing views have been offered on the direction of the surface temperature gradient. Deegan *et al*. [2] believed the apex of the droplet to be coolest due to its longer conduction distance from the substrate, which leads to a positive (i.e., outward) radial temperature gradient along the droplet surface. Contrarily, Steinchen and Sefiane [42] assumed that the edge of the droplet is colder because of the larger evaporation rate at this edge, and thus the surface temperature gradient is negative (i.e., inward). Theoretical predictions [4,6,43] and infrared thermographic observations [44,45] showed that the surface temperature of drying droplets on isothermal substrates will increase monotonically from the center to the edge, which constitutes a positive surface temperature gradient. However, numerical simulations by Hu and Larson [23] showed that the radial surface temperature gradient of drying drops on finite thickness substrates will reverse its direction at a critical contact angle. Further analyses by Ristenpart *et al*. [6] and Xu *et al*. [4] indicated that the critical contact angle is determined both by the relative thermal conductivities of the substrate and the liquid and by the ratio of the substrate thickness to the contact line radius of the droplet.

Despite the differences in the direction of the surface temperature gradient, the above studies all assumed a monotonic temperature profile along the droplet surface. However, we show here that this assumption only partly explains the phenomenon and that a nonmonotonic spatial dependence of the surface temperature may appear. By numerically solving the temperature fields of drying droplets resting on flat substrates, the patterns of the temperature distribution along the droplet surface are analyzed and then explained by combining the effect of the evaporative cooling and the effect of the heat conduction. The influences of the relative thermal conductivities of the substrate and the liquid on the surface temperature are also discussed. Furthermore, a "phase diagram" for the temperature distribution along the droplet surface is introduced, and the influence of the temperature distribution on the flow field inside the droplet is also discussed. The present study may contribute to the body of knowledge concerning the Marangoni effects in evaporating liquid droplets and thus may be useful to predict and control the flow field and the deposition pattern of drying droplets.

*Corresponding author: xuxuefeng@bjfu.edu.cn

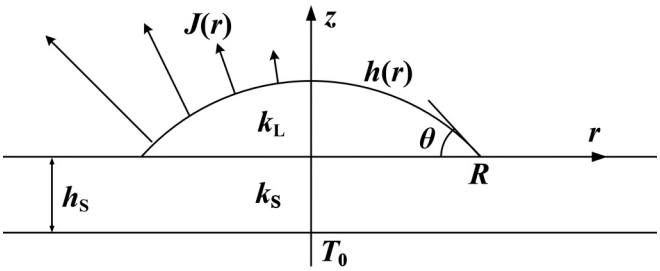

FIG. 1. A sessile spherical-cap liquid droplet on a flat substrate in a cylindrical coordinate system with radial coordinate r and axial coordinate z.

II. MATHEMATIC MODEL

Here, we consider a small, pinned, and slowly evaporating liquid droplet with a contact angle of θ ($0 < \theta < \pi/2$) and contact line radius of R resting on a flat substrate of thickness h_S (Fig. 1). The thermal conductivities of the substrate and the liquid are k_S and k_L, respectively. The temperature at the lower surface of the substrate is fixed at T_0. Due to the axisymmetric configuration, a cylindrical coordinate system (r, z) is chosen.

For the pinned, and slowly evaporating droplets, the evaporation flux along the droplet surface can be well approximated by the simple form $J(r) = J_0(\theta)(1 - r^2/R^2)^{-\lambda(\theta)}$, where $\lambda(\theta) = (1/2–\theta/\pi)$, $J_0(\theta) = J_0(\pi/2)(0.27\theta^2 + 1.30)[0.6381 - 0.2239(\theta - \pi/4)^2]$, $J_0(\pi/2) = D(1 - H)c_v/R$, D is the water vapor diffusivity, c_v is the saturated water vapor concentration, and H is the relative humidity [1,2,27]. By estimating the ratio of the relative rates of change of droplet height to that of temperature, Hu and Larson [23] showed that the temperature field in the drying droplet is at quasisteady state. The thermal energy equation in the droplets is then $\mathrm{Pe}\boldsymbol{u}\cdot\nabla T + \nabla^2 T = 0$, where $\boldsymbol{u}$ is the liquid velocity, and the Peclet number Pe is a ratio of the convective to the conductive heat transfer [6]. Typically $\mathrm{Pe} \ll 1$, implying that the rate of the convective heat transfer is much smaller than that of the conductive one in the drying droplets [6,23]. Ristenpart *et al.* [6] further indicated that, although the velocity $\boldsymbol{u}$ diverges in the vicinity of the contact line, conduction is nonetheless dominant in the whole droplet. Therefore, inside the slowly evaporating droplets, the temperature field can be governed by Laplace's equation [6,23,28,29], which can be written in a nondimensional form as follows [4,43]:

$$\widetilde{\nabla}^2\widetilde{T} = 0, \tag{1}$$

where $\widetilde{\nabla}^2 = \frac{\partial^2}{\partial\tilde{r}^2} + \frac{1}{\tilde{r}}\frac{\partial}{\partial\tilde{r}} + \frac{\partial^2}{\partial\tilde{z}^2}$, $\tilde{r} = r/R$, $\tilde{z} = z/R$, $\widetilde{T} = \frac{(T-T_0)k_L}{H_L J_0 R}$ is the dimensionless temperature, and H_L is the latent heat of evaporation.

The nondimensional boundary conditions for Eq. (1) are as follows [4,43]:

$$-\widetilde{\nabla}\widetilde{T}_L\cdot\boldsymbol{n} = (1-\tilde{r}^2)^{-(1/2-\theta/\pi)} \quad \text{at} \quad \tilde{z} = \widetilde{h}(\tilde{r}), \quad 0 \leqslant \tilde{r} \leqslant 1, \tag{2}$$

$$\widetilde{\nabla}\widetilde{T}_S\cdot\boldsymbol{n} = 0 \quad \text{at} \quad \tilde{z} = 0, \quad \tilde{r} > 1, \tag{3}$$

$$\widetilde{T}_L = \widetilde{T}_S, \quad \widetilde{\nabla}\widetilde{T}_L\cdot\boldsymbol{n} = k_R\widetilde{\nabla}\widetilde{T}_S\cdot n \quad \text{at} \quad \tilde{z} = 0, \quad 0 \leqslant \tilde{r} \leqslant 1, \tag{4}$$

$$\widetilde{T}_S = 0, \quad \text{at} \quad \tilde{z} = -h_R; \quad -h_R < \tilde{z} < 0, \quad \tilde{r} \to \infty, \tag{5}$$

where $\widetilde{\nabla} = e_{\mathbf{r}}\frac{\partial}{\partial\tilde{r}} + e_{\mathbf{z}}\frac{\partial}{\partial\tilde{z}}$, $\boldsymbol{e_r}$ is the radial unit vector, $\boldsymbol{e_z}$ is the axial unit vector, $\boldsymbol{n}$ is the unit normal, $\widetilde{T}_L$ is the dimensionless temperature in the liquid, $\widetilde{T}_S$ is the dimensionless temperature in the substrate, $\widetilde{h}(\tilde{r}) = h(r)/R = \sqrt{1/\sin^2\theta - \tilde{r}^2} - 1/\tan\theta$, $h(r)$ is the height of the droplet, $k_R = k_S/k_L$ is the relative thermal conductivity, and $h_R = h_S/R$ is the relative substrate thickness.

III. FINITE ELEMENT METHOD

By incorporating the boundary conditions listed in Eqs. (2)–(5), Eq. (1) can be numerically solved using a commercial software, ANSYS (Ansys, Inc). In the finite element method (FEM) models, the radius of the substrate is taken to be $1.5R$ because the results are insensitive to further increases in the radius. When the contact angle of the droplet is less than 5°, an error stating that a topological degeneracy has been detected will occur in the modeling process of the simulations. Thus, the contact angle, θ, in the present calculations is chosen in the range $5° \leq \theta < 90°$ to ensure the accuracy of the numerical results.

To obtain an accurate surface temperature distribution, the mesh in the model is refined continuously until the criterion

$$\varepsilon = \left(\widetilde{T}_i|_{\tilde{r}}^{n+1} - \widetilde{T}_i|_{\tilde{r}}^{n}\right)\Big/\widetilde{T}_i|_{\tilde{r}}^{n+1} < 0.005 \quad (\tilde{r} \leqslant 0.95) \tag{6}$$

is satisfied, where $\widetilde{T}_i|_{\tilde{r}}^{n}$ is the dimensionless surface temperature at $\tilde{r}$ for the nth finite element mesh refinement.

The influence of the refinement on the numerical results is shown in Fig. 2, which indicates that the distribution of the surface temperature is nonmonotonic: The surface temperature first decreases from the center to the edge of the droplet, reaches its lowest value, and then increases again. From the figure it can also be seen that while the convergence criterion in Eq. (6) is satisfied in the central region of the droplet, the criterion cannot be achieved in the region near the droplet edge as the refinement proceeds. This problem arises from a

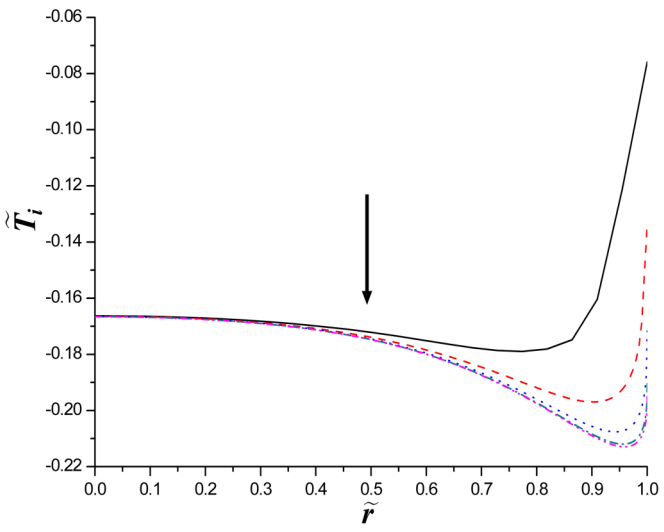

FIG. 2. (Color online) Influence of the refinement on the surface temperature of drying droplet. The black arrow indicates the direction of the refinement progress. The parameters used are as follows: $k_R = 2$, $h_R = 0.2$, and $\theta = 7°$.

mathematical issue. In the present model, the evaporation flux becomes singular when approaching the droplet edge and two kinds of boundary conditions meet at the edge, and as a result, convergence of the computation may not be achieved in the region close to the contact line even though the mesh is further refined.

Thus, we restrict our analysis to the surface temperature in the central region of the droplet. In the computation, the convergence criterion used here can ensure that the obtained temperature is accurate on most of the droplet surface (i.e., in the region $\tilde{r} \leqslant 0.95$). In the following text, the velocity field in the droplets is computed by using a lubrication theory developed by Hu and Larson [23,28]. In the lubrication theory, the liquid velocity in the droplet is related only to the local surface temperature gradient. This means that the flow field computed by the lubrication theory is also accurate in most of the droplet (i.e., in the region $\tilde{r} \leqslant 0.95$).

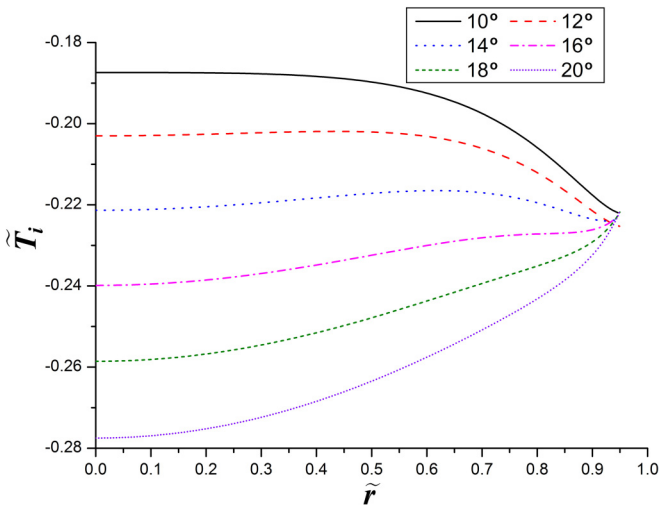

FIG. 3. (Color online) The dimensionless surface temperature, $\widetilde{T}_i$, of a drying droplet at contact angles of 10°, 12°, 14°, 16°, 18°, and 20° computed by the finite element method. The parameters used are as follows: $k_R = 1.5806$ for water droplets on glass substrates, and $h_R = 0.15$.

IV. RESULTS AND DISCUSSION

A. Patterns of the surface temperature distribution

Let us first analyze the distribution of the surface temperature of a pinned liquid droplet drying on a planar substrate (see Fig. 1). During the evaporation, the radial surface temperature gradient of the droplet reverses its direction at the critical contact angle, θ_{Crit}. Therefore, if the temperature distribution along the droplet surface is always monotonic, the temperature must be uniform over the surface when $\theta = \theta_{\text{Crit}}$. Considering the spherical-cap shape of the droplets, a uniform temperature over the droplet surface for all the values of θ, R, h_S, k_S, and k_L is not so reasonable. This implies that the surface temperature may change nonmonotonically during the transition period, i.e., when the contact angle is near the critical value, θ_{Crit}.

We will then corroborate the above assertion by numerically solving the temperature field inside the drying droplets. The nondimensional equations (1)–(5) clearly indicate that the temperature fields in the droplets are governed by three parameters: k_R, h_R, and θ. Here, the parameters are chosen as follows: The relative substrate thickness is $h_R = 0.15$, the thermal conductivity of water is $k_L = 1.4536 \times 10^{-3}$ (cal cm^{-1} s^{-1} K^{-1}) [23], and the thermal conductivity of glass is $k_S = 2.2976 \times 10^{-3}$ (cal cm^{-1} s^{-1} K^{-1}) [23]. Thus, the relative thermal conductivity is $k_R = 1.5806$. The contact angles of the droplets are 10°, 12°, 14°, 16°, 18°, and 20°, which are near the critical value of 14° obtained by Hu and Larson [23].

By using the above parameters, the dimensionless surface temperature, $\widetilde{T}_i$, is obtained as a function of $\tilde{r}$ for drying water droplets and plotted in Fig. 3. The figure clearly shows that the gradient of the surface temperature reverses its direction as the contact angle decreases, and the distribution of the surface temperature becomes nonmonotonic in the transition period. The figure indicates that three states of the surface temperature distribution will appear as the contact angle changes: (i) at a contact angle above 16°, the surface temperature increases monotonically from the center to the edge of the droplet; (ii) at a contact angle between 12° and 16°, the temperature exhibits a nonmonotonic spatial dependence along the droplet surface: It first increases and then decreases from the top to the edge of the droplet; (iii) at a contact angle below 12°, the surface temperature decreases monotonically from the center to the edge of the droplet.

Thinking in terms of the synergy between the evaporative cooling at the droplet surface and the heat conduction across the substrate and the liquid helps to understand these surface temperature profiles. During evaporation, evaporative cooling reduces the liquid temperature at the droplet surface. To compensate for the evaporative heat loss and to maintain the liquid temperature necessary for evaporation, heat is transferred from the lower surface of the substrate to the droplet surface by conduction in the substrate and in the liquid. Hence, the surface temperature is mainly determined by two factors: the evaporation rate at the surface and the heat conduction path length to the surface.

For given values of k_R and h_R, the relative influence of the evaporation rate and the conduction path length on the surface temperature is determined by the value of the contact angle, θ. When the contact angle is large, the difference in the conduction path length is comparatively remarkable, and the nonuniformity in the evaporation rate is relatively undetectable along the droplet surface [1,2,27]. Thus, the surface temperature is more likely dominated by the conduction path length and will then increase monotonically from the droplet center where the heat conduction distance is the longest to the droplet edge where the conduction path is the shortest. Contrarily, the difference in the conduction path length can be neglected for small contact angles, and the nonuniformity in the evaporation rate is comparatively apparent. Therefore, the evaporative cooling effect may be predominant, and the surface temperature then decreases monotonically from the droplet center where the evaporation rate is the lowest to the droplet edge where the evaporation rate is the highest. For the intermediate contact angles, the influences of the evaporative cooling and the conduction path are comparable. Hence, the surface temperature exhibits a nonmonotonic spatial distribution.

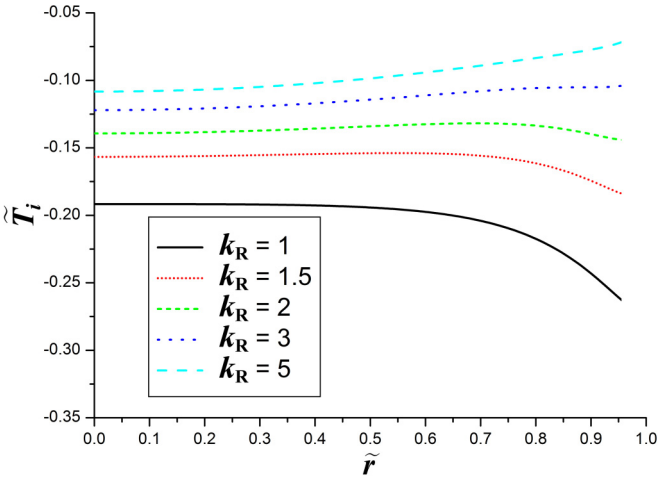

FIG. 4. (Color online) The dimensionless surface temperature, $\widetilde{T}_i$, of a drying droplet at relative thermal conductivities of 1, 1.5, 2, 3, and 5. The parameters used are as follows: $h_R = 0.1$ and $\theta = 10°$.

B. Influence of k_R on surface temperature distribution

The thermal conductivities of the substrate and the liquid significantly affect the temperature field of drying droplets. The asymptotic analyses by Ristenpart *et al.* [6] and by Xu *et al.* [4] indicated that the critical contact angle is closely related to the relative thermal conductivities of the substrate and the liquid. To investigate the influence of the relative thermal conductivity, k_R, on the spatial distribution of the surface temperature, the dimensionless surface temperature, $\widetilde{T}_i$, is obtained as a function of $\tilde{r}$ for drying droplets on substrates with different thermal conductivities and then plotted in Fig. 4.

Figure 4 shows that the above-mentioned profiles of the surface temperature also appear successively as k_R changes: For sufficiently large values of k_R, the surface temperature increases with the distance from the top of the droplet; for small k_R, the surface temperature decreases with the distance from the top of the droplet; and for intermediate values of k_R, the spatial distribution of the surface temperature is nonmonotonic.

The effects of k_R on the spatial distribution of the surface temperature can also be explained by combining the evaporative cooling and the conduction path length. For conductive substrates with a high thermal conductivity, the length of the conduction path through the substrates can be neglected compared with that in the liquid. As a result, the difference in the path lengths is relatively notable along the droplet surface due to the spherical-cap shape of the droplet. In this case, the surface temperature is most likely dominated by the length of the conduction path. In contrast, the lengths of the conduction path are almost identical along the droplet surface for insulating substrates with low thermal conductivity because the path length in the liquid can be neglected compared with that in the substrate. In this situation, the surface temperature should be determined by the evaporation rate at the surface. For intermediate k_R values, the evaporative cooling effect and the heat conduction effect are comparable, which results in a nonmonotonic temperature distribution along the surface.

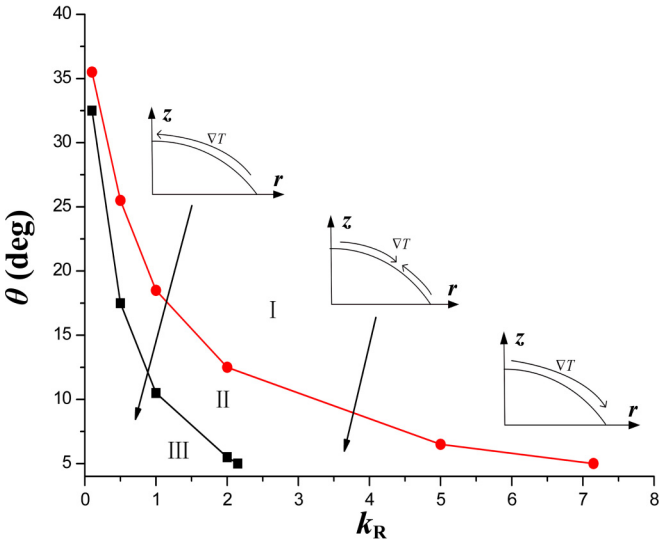

FIG. 5. (Color online) "Phase diagram" for the temperature distribution along the surface of drying droplet on substrates with the relative thickness of $h_R = 0.1$. The data points were obtained from numerical simulations.

C. "Phase diagram" for the surface temperature distribution

The patterns of the surface temperature distribution can be summarized in a "phase diagram" on the parameter plane (k_R, θ). As shown in Fig. 5, the phase plane is divided into three regions, i.e., region I, where the surface temperature increases monotonically from the center to the edge of the droplet; region II, where the temperature exhibits a nonmonotonic spatial dependence along the droplet surface; and region III, where the surface temperature decreases monotonically from the center to the edge of the droplet.

Figure 5 also shows that the surface temperature of pinned drying droplets can undergo all three states as the contact angle decreases during evaporation for small values of k_R (approximately $k_R \leqslant 2.5$). However, only two patterns of surface temperature can be observed on the droplet surface for intermediate values of k_R from 2.5 to 7.5. Therefore, the inward (or negative) temperature gradient will not appear on the droplet surface on substrates with intermediate thermal conductivity. Thus, the droplet is unlikely to contain convective Marangoni flow, which is radially inward along the substrate and radially outward along the air-liquid interface. For large k_R (approximately $k_R \geqslant 7.5$), the surface temperature will increase monotonically from the center to the edge of the droplet throughout the evaporation process, which is similar for isothermal substrates.

The "phase number" decreases because the significance of the effect of evaporative cooling decreases relative to the effect of the conduction path length as the thermal conductivity of the substrate increases. When the evaporative cooling effect is too weak to dominate, the inward temperature gradient will no longer appear on the droplet surface. If the thermal conductivity of the substrate is sufficiently high, the effect of the conduction path length will be predominant during the entire evaporation process. As a result, the surface temperature always increases with the distance from the top of the droplet.

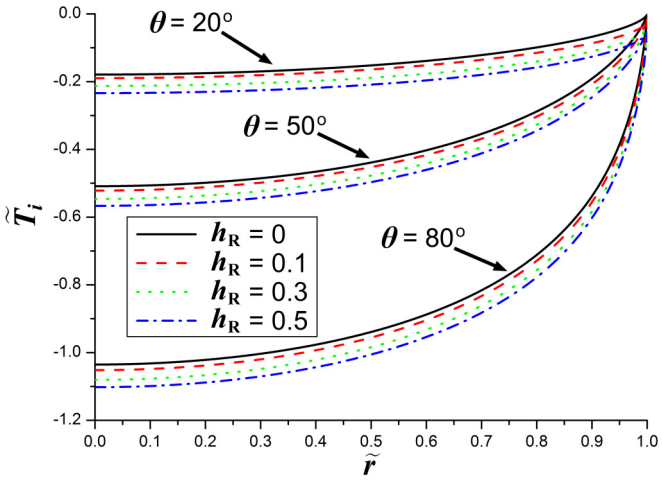

FIG. 6. (Color online) The dimensionless surface temperature, $\widetilde{T}_i$, of drying droplets on substrates with a relative thermal conductivity of $k_R = 10$.

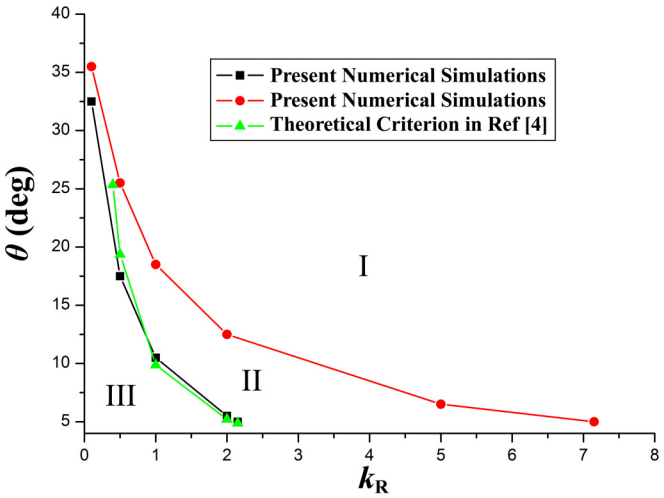

FIG. 7. (Color online) Comparison between the present numerical simulations and the previous theoretical analyses. The relative thickness of the substrates $h_R = 0.1$.

The surface temperature of liquid droplets drying on flat substrates with a relative thermal conductivity of $k_R = 10$ is numerically solved and plotted in Fig. 6. The figure shows that the surface temperature always increases from the center to the edge of the droplet for $k_R = 10$, and its spatial profiles along the surface of finite thickness substrates are quite close to that of isothermal substrates (i.e., $h_R = 0$). This conformity in the distribution of the surface temperature implies that a substrate with a k_R exceeding 10 can be reasonably assumed as isothermal, especially when the substrate is thin.

D. Comparison with the previous theory

A quantitative criterion for the direction of the surface temperature gradient of drying droplets was established in our previous paper based on an asymptotic analysis of the heat transfer in the droplet central region [4]. To compare the present "phase diagram" with the quantitative criterion in the previous paper, the critical contact angles are calculated according to the criterion and then plotted in Fig. 7 together with the data from the present numerical computations. These two theories both suggest that the surface temperature increases (decreases) with distance from the top of the droplet for large (small) values of contact angle θ. As shown in Fig. 7, the critical contact angles at which the radial temperature gradient along the surface exhibits a transition to a negative slope are almost the same in the two theories. This consistency may partly corroborate the validity of both the numerical simulations in the present work and the theoretical analyses in the previous theory.

The difference between these two theories is that a region containing a nonmonotonic spatial dependence of the temperature does not appear in the phase plane given by the previous criterion. This difference is attributed to the assumption of a monotonously changing surface temperature, which results in only the surface temperature close to the symmetry axis being analyzed in the previous model. Although a nonmonotonic distribution of the surface temperature appears, the theories presented by Hu and Larson [23], Ristenpart *et al.* [6], and Xu *et al.* [4] are still applicable in most cases because the surface temperature of drying droplets still varies monotonically when the contact angle is not close to the critical value (see Fig. 7).

E. Effect of surface temperature distribution on flow structure

Hu and Larson [23,28] have developed a lubrication theory to obtain an analytical solution for the velocity in the drying droplets. They showed that the lubrication approximation provides an accurate analytical solution to the flow field of drying droplets. Here, with the numerical results of the surface temperature obtained above, we have computed the velocity field in the droplets by using the lubrication analysis method.

To show the effect of the temperature distribution along the droplet surface on the flow structure within the droplet, the velocity fields of drying droplets at three contact angles of 10°, 14°, and 18° are illustrated in Fig. 8. From the figure it can be seen that the surface temperature distribution has significant influence on the flow structure inside the droplets. When the distribution of the surface temperature is monotonic, a single vortex flow structure often appears inside the droplet (at contact angles of 10° and 18°). Contrarily, a two-vortex flow structure may emerge in the droplet when the variation of the surface temperature is nonmonotonic (at contact angle of 14°).

The structures of the flow field in drying droplets can be explained by the Marangoni stress along the droplet surface generated by the nonuniform surface temperature. When the surface temperature decreases (increases) monotonically from the center to the edge of the droplet, an outward (inward) stress along the droplet surface will form because, for most liquids, the surface tension decreases with rising temperature. This stress will generate a clockwise (counterclockwise) circulation inside the droplet [4–6,23]. If the distribution of the surface temperature is nonmonotonic, e.g., the surface temperature increases first and then decreases as one moves from the center to the edge of the droplet with a contact angle of 14°,

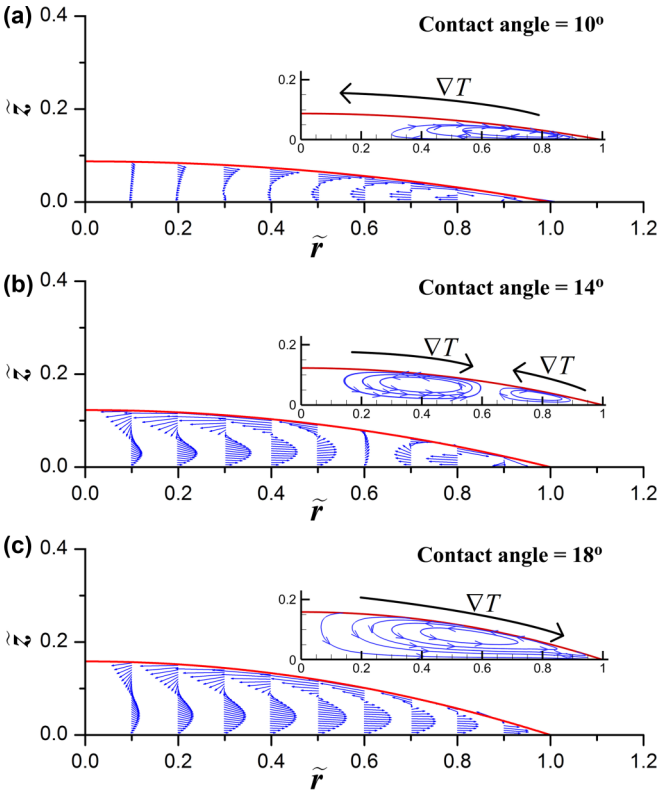

FIG. 8. (Color online) The sketch of the velocity fields in the drying droplet at contact angles of (a) 10°, (b) 14°, and (c) 18°, calculated by using the lubrication theory developed by Hu and Larson [23,28]. The insets in each panel show the streamlines of the flow fields inside the drying droplets and the direction of the temperature gradient along the droplet surface.

a Marangoni stress which is inward in the central region and becomes outward in the outer region of the droplet is induced along the droplet surface. Such a Marangoni stress may generate two vortexes inside the droplet: a counterclockwise vortex in the central region and a clockwise one in the outer region as shown in Fig. 8(b).

V. CONCLUSIONS

We first performed an analysis on the surface temperature of drying liquid droplets, which demonstrates that the spatial distribution of the temperature along the droplet surface may be nonmonotonic. To corroborate this assertion, the temperature field inside evaporating liquid droplets resting on flat substrates has been numerically solved. The results indicated that three different distributions of the surface temperature will appear as the contact angle decreases during the evaporation process: (i) the surface temperature increases monotonically from the center to the edge of the droplet; (ii) the surface temperature exhibits a nonmonotonic spatial distribution along the droplet surface; (iii) the surface temperature decreases monotonically from the center to the edge of the droplet. These patterns of the surface temperature distribution have been explained by combining the evaporative cooling at the droplet surface and the heat conduction across the substrate and the liquid. The influence of the relative thermal conductivities of the substrate and the liquid on the surface temperature distribution has been discussed. Then, a "phase diagram" for the surface temperature distribution was presented and further discussions indicated that the surface temperature distribution has significant influences on the flow field inside the droplets.

The "phase diagram" was also compared and found consistent with the previous theoretical criterion. Despite its simple origin and limitations, the results presented in this study may serve as an attempt to understand thoroughly the spatial distribution of the surface temperature and the Marangoni effect of drying droplets. Thus, they may provide a potential way to predict and control the flow field and the deposition of drying droplets.

ACKNOWLEDGMENTS

The work is financially supported by the Program for New Century Excellent Talents in University (Grant No. NCET-12-0786), the National Natural Science Foundation of China (Grant No. 51275050), and the Specialized Research Fund for the Doctoral Program of Higher Education (Grant No. 20120014120017).

[1] R. D. Deegan, O. Bakajin, T. F. Dupont, G. Huber, S. R. Nagel, and T. A. Witten, Nature **389**, 827 (1997).
[2] R. D. Deegan, O. Bakajin, T. F. Dupont, G. Huber, S. R. Nagel, and T. A. Witten, Phys. Rev. E **62**, 756 (2000).
[3] R. D. Deegan, Phys. Rev. E **61**, 475 (2000).
[4] X. F. Xu, J. B. Luo, and D. Guo, Langmuir **26**, 1918 (2010).
[5] H. Hu and R. G. Larson, J. Phys. Chem. B **110**, 7090 (2006).
[6] W. D. Ristenpart, P. G. Kim, C. Domingues, J. Wan, and H. A. Stone, Phys. Rev. Lett. **99**, 234502 (2007).
[7] G. Berteloot, A. Hoang, A. Daerr, H. P. Kavehpour, F. Lequeux, and L. Limat, J. Colloid Interface Sci. **370**, 155 (2012).
[8] B. M. Weon and J. H. Je, Phys. Rev. E **82**, 015305(R) (2010).
[9] M. Schena, D. Shalon, R. W. Davis, and P. O. Brown, Science **270**, 467 (1995).
[10] M. Schena, D. Shalon, R. Heller, A. Chai, P. O. Brown, and R. W. Davis, Proc. Natl. Acad. Sci. USA **93**, 10614 (1996).
[11] J. P. Jing, J. Reed, J. Huang, X. H. Hu, V. Clarke, J. Edington, D. Housman, T. S. Anantharaman, E. J. Huff, B. Mishra, B. Porter, A. Shenker, E. Wolfson, C. Hiort, R. Kantor, C. Aston, and D. C. Schwartz, Proc. Natl. Acad. Sci. USA **95**, 8046 (1998).
[12] T. Sekitani, Y. Noguchi, U. Zschieschang, H. Klauk, and T. Someya, Proc. Natl. Acad. Sci. USA **105**, 4976 (2008).
[13] J. Park and J. Moon, Langmuir **22**, 3506 (2006).
[14] T. Kawase, H. Sirringhaus, R. H. Friend, and T. Shimoda, Adv. Mater. **13**, 1601 (2001).
[15] H. Sirringhaus, T. Kawase, R. H. Friend, T. Shimoda, M. Inbasekaran, W. Wu, and E. P. Woo, Science **290**, 2123 (2000).
[16] J. R. E. Christy, K. Sefiane, and E. Munro, J. Bionic Eng. **7**, 321 (2010).
[17] Y. Cai and B. Z. Newby, J. Am. Chem. Soc. **130**, 6076 (2008).
[18] L. Yu. Barash, T. P. Bigioni, V. M. Vinokur, and L. N. Shchur, Phys. Rev. E **79**, 046301 (2009).
[19] F. Duan and C. A. Ward, Langmuir **25**, 7424 (2009).

[20] F. Duan, J. Phys. D: Appl. Phys. **42**, 102004 (2009).
[21] N. Murisic and L. Kondic, J. Fluid Mech. **679**, 219 (2011).
[22] X. F. Xu and J. B. Luo, Appl. Phys. Lett. **91**, 124102 (2007).
[23] H. Hu and R. G. Larson, Langmuir **21**, 3972 (2005).
[24] C. A. Ward and F. Duan, Phys. Rev. E **69**, 056308 (2004).
[25] B. D. MacDonald and C. A. Ward, J. Colloid Interface Sci. **383**, 198 (2012).
[26] M. Kaneda, Y. Takao, and J. Fukai, Int. J. Heat Mass Transfer **53**, 4448 (2010).
[27] H. Hu and R. G. Larson, J. Phys. Chem. B **106**, 1334 (2002).
[28] H. Hu and R. G. Larson, Langmuir **21**, 3963 (2005).
[29] F. Girard, M. Antoni, and K. Sefiane, Langmuir **24**, 9207 (2008).
[30] K. Sefiane, S. K. Wilson, S. David, G. J. Dunn, and B. R. Duffy, Phys. Fluids **21**, 062101 (2009).
[31] G. J. Dunn, S. K. Wilson, B. R. Duffy, and K. Sefiane, Phys. Fluids **21**, 052101 (2009).
[32] H. Ghasemi and C. A. Ward, Phys. Rev. Lett. **105**, 136102 (2010).
[33] Y. Hamamoto, J. R. E. Christy, and K. Sefiane, Phys. Rev. E **83**, 051602 (2011).
[34] H. Y. Erbil, Adv. Colloid Interface Sci. **170**, 67 (2012).
[35] B. Sobac and D. Brutin, Phys. Fluids **24**, 032103 (2012).
[36] H. Ghasemi and C. A. Ward, J. Phys. Chem. C **115**, 21311 (2011).
[37] A. J. Petsi and V. N. Burganos, Phys. Rev. E **84**, 011201 (2011).
[38] S. A. Putnam, A. M. Briones, L. W. Byrd, J. S. Ervin, M. S. Hanchak, A. White, and J. G. Jones, Int. J. Heat Mass Transfer **55**, 5793 (2012).
[39] M. A. Saada, S. Chikh, and L. Tadrist, Phys. Fluids **22**, 112115 (2010).
[40] G. J. Dunn, S. K. Wilson, B. R. Duffy, S. David, and K. Sefiane, J. Fluid Mech. **623**, 329 (2009).
[41] F. Girard and M. Antoni, Langmuir **24**, 11342 (2008).
[42] A. Steinchen and K. Sefiane, J. Non-Equilib. Thermodyn. **30**, 39 (2005).
[43] X. F. Xu, J. B. Luo, and D. Guo, Soft Matter **8**, 5797 (2012).
[44] F. Girard, M. Antoni, and K. Sefiane, Langmuir **26**, 4576 (2010).
[45] F. Girard, M. Antoni, and K. Sefiane, Langmuir **27**, 6744 (2011).